KURENAI
Kyoto University Research Information Repository

KYOTO UNIVERSITY

Title	Accuracy of reaction rates in the accelerator-driven system with 14MeV neutrons at the Kyoto University Critical Assembly
Author(s)	Pyeon, Cheol Ho; Takemoto, Yuki; Yagi, Takahiro; Lim, Jae-Yong; Takahashi, Yoshiyuki; Misawa, Tsuyoshi
Citation	Annals of Nuclear Energy (2012), 40(1): 229-236
Issue Date	2012-02
URL	http://hdl.handle.net/2433/152380
Right	© 2011 Elsevier Ltd.
Type	Journal Article
Textversion	author

Kyoto University

Accuracy of reaction rates in the accelerator-driven system with 14 MeV neutrons at the Kyoto University Critical Assembly

Cheol Ho Pyeon[1*], Yuki Takemoto[2], Takahiro Yagi[1], Jae-Yong Lim[1]

Yoshiyuki Takahashi[1] and Tsuyoshi Misawa[1]

[1]*Nuclear Engineering Science Division, Research Reactor Institute, Kyoto University,*

Asashiro-nishi, Kumatori-cho, Sennan-gun, Osaka 590-0494, Japan

[2]*Department of Fundamental Energy Science, Graduate School of Energy Science, Kyoto*

University, Yoshida-honmachi, Sakyo-ku, Kyoto, 606-8501, Japan

Reaction rate experiments on the accelerator-driven system (ADS) are conducted by combining a critical assembly of a solid-moderated and -reflected core with a pulsed neutron generator. Neutrons (14 MeV) generated from the accelerator are injected into a subcritical system and the reaction rates are measured by the foil activation method to obtain neutronic spectrum data. The numerical calculations are executed by MCNPX with ENDF/B-VI.8, JENDL-3.3 and JENDL/D-99 libraries to evaluate the reaction rates of activation foils set in the center of the core. For the ADS experiments with 14 MeV neutrons, the C/E values between the experiments and the calculations are found to be well within the relative difference of about 30% in all foils up to subcriticality 1.05 %$\Delta k/k$. The reaction rates don't depend on the subcriticality level in cases of ^{115}In, ^{56}Fe (purity 99.99%), ^{27}Al, whereas subcriticality dependence is observed in ^{93}Nb. In the critical experiments carried out in the A, B and C cores, special mention should be made of the remarkable effect of the composition rate of ^{56}Fe material. Thus a remarkable improvement is observed in the accuracy of experimental and numerical reaction rates, demonstrating the importance of material impurity

---

[*] Corresponding author, Tel.: +81-72-451-2356; fax: +81-72-451-2603;
E-mail address: pyeon@rri.kyoto-u.ac.jp (C.H. Pyeon)

for subcritical experiments.

2

1. Introduction

The accelerator-driven system (ADS) was first proposed as an energy amplifier system (Rubbia, 1995) that couples with a high-power accelerator and a thorium sustainable system. Another possible function of ADS was resolving the issue of the treatment of minor actinides (MAs) and long-lived fission products (LLFPs) from nuclear power plants. While numerical simulations were executed by the deterministic and stochastic approaches (Nishihara et al., 2008; Sugawara et al., 2010; 2011) regarding the evaluation of MAs and LLFPs burning in ADS, the current research activities on ADS involved mainly the experimental feasibility study using critical assemblies and test facilities: MASURCA (Soule et al., 2004; Plaschy et al., 2005; Lebrat et al., 2008), YALINA-booster and -thermal (Persson et al., 2008; Gohar et al., 2009; Tesinsky et al., 2011), VENUS-1 (Xia, 2009), and the Kyoto University Critical Assembly (KUCA) (Pyeon et al., 2007; 2008; 2009a; 2009b; 2010; Taninaka et al., 2010; 2011). The new ADS test facility of GUINEVERE (Uyttenhove et al., 2011) is being commissioned to start actual operation in subcritical states after the first critical experiments.

At the ADS facilities, reactor physics experiments were carried out to investigate neutronic characteristics through the measurements of several reactor physics parameters, including reaction rates, neutron spectrum, neutron multiplication (k-source), subcriticality and delayed neutron decay constants. Among these, the neutron spectrum was considered an important parameter for recognizing information on neutron energy in the core. In the MUSE experiments at MASURCA, neutron spectrum analyses were conducted experimentally by the foil activation method, and pertinent data revealed the importance of the following items: uncertainties associated with the cross section of the high-energy threshold, the exact location of the external source, the subcriticality level, the correct modeling at external anisotropy and spectrum change. At KUCA, from the importance experiences in the MUSE experiments, additional experimental analyses (Pyeon et al., 2009b) focused on the reaction rates, by the foil activation method, for the subcriticality change: while the accuracy of the reaction rates was not satisfied within the allowance of error

between experiments and calculations, subcriticality dependence was demonstrated in reaction rate analyses, through the ADS experiments with 14 MeV neutrons. Moreover, through the experimental and numerical analyses in the YALINA-booster with 14 MeV neutrons, some difficulty (Tesinsky et al., 2011) of precise reaction rates by MCNP (Team, 2005) was revealed in subcritical systems.

In previous KUCA experiments, a large discrepancy between the experimental and numerical reaction rates was found in the ADS with 14 MeV neutrons. Here, to resolve this discrepancy, first, special attention was paid to the reaction rate analyses of the critical state and the characteristics of some nuclei in activation foils: the composition ratio of material. The reaction rate experiments were carried out in the critical state at the KUCA A-core and B-core (polyethylene-moderated and -reflected core) and C-core (water-moderated and -reflected core; Pyeon et al., 2004). Second, on the basis of the critical experiments, the ADS experiments with 14 MeV neutrons were conducted in the A-core, as in previous ADS experiments with 14 MeV neutrons; however, the neutron spectrum was different. On the other hand, a neutron guide and a beam duct (Pyeon et al., 2007; 2008) were installed in the previous study to direct the highest number of neutrons generated at the tritium target, since the target is located outside the core. Furthermore, a large size of activation foils was employed to attain a large number of γ-ray emission counts at the void region in the center of the core. While the effect of the neutron guide and the beam duct was experimentally demonstrated to be valid from the viewpoint of neutron transportation from the target to the core center, an uncertainty factor caused by a large perturbation (large void region in the core center) was induced by the installation of the neutron guide and the beam duct in the experimental analyses. In this study, the neutron guide and the beam duct were not installed for eliminating the uncertainty factor; efforts were made in the core configuration for achieving attachment of the core to the external source and attaining as high neutron flux and as much reactor power as possible in the core. As a result, a small size of activation foils was possibly employed to exclude the uncertainty factors (self-shielding and source volume;

Pyeon et al., 2009b) evaluated in previous study.

The objective of this study was to examine the accuracy of reaction rates in the ADS experiments with 14 MeV neutrons, although the neutron spectrum was relatively hard in the polyethylene-moderated and -reflected core, as compared with previous studies. The neutron spectrum experiments with 14 MeV neutrons generated by deuteron-tritium (D-T) reactions are shown in Sec. 2 and include descriptions of the core configuration and experimental settings. The results of numerical analyses by the Monte Carlo calculation code MCNPX (Hendricks et al., 2005) combined with nuclear data libraries are presented in Sec. 3 and the conclusions are summarized in Sec. 4.

2. Reaction Rate Experiments

2.1. Core Configuration

At KUCA, A and B are polyethylene-moderated and -reflected cores, and C is a light water-moderated and -reflected one. The three cores are operated at a low mW power in the normal operating state; the maximum power is 100 W. The critical experiment for the reaction rates was carried out in the B-core (B3/8"P36EU(3); Fig. 1), which has fuel and polyethylene reflector rods (Fig. 2). In the B-core, the fuel assembly is composed of 36 unit cells, and upper and lower polyethylene blocks about 591 and 537 mm long, respectively, in an aluminum (Al) sheath $54 \times 54 \times 1520$ mm^3. For the fuel assembly, a unit cell in the fuel region is composed of a highly-enriched uranium fuel plate 1/16" thick, polyethylene plates 1/8" and 1/4" thick. In the C-core (C35G0(5); Fig. 3), the fuel region ($284 \times 303 \times 735$ mm^3) comprises ten and five fuel assemblies loading 40 and 5 fuel plates, respectively, and the core is surrounded by light water. The fuel plate is a highly-enriched uranium plate 600 mm long, 62 mm wide and 1.5 mm thick with Al cladding 0.5 mm thick.

In the A-core (A1/8"P60EU-EU(3); Fig. 4), the normal fuel assembly (Fig. 5a) is composed of 60 unit cells, and upper and lower polyethylene blocks about 561 and 548 mm

long, respectively, in an Al sheath $54 \times 54 \times 1520$ mm^3 as in the B-core.   For the normal and partial fuel (Fig. 5b) assemblies, a unit cell in the fuel region is composed of a highly-enriched uranium fuel plate 1/8'' (1/16''$\times$2) and a polyethylene plate 1/8'' thick.   The numeral 28 corresponds to the number of fuel plates in the partial fuel assembly used for reaching criticality mass.   The tritium target is located outside the core and is not easily moved to the center of the core because the control and safety rods are fixed in the core as the control driving system.

2.2. Experimental Settings

In the critical experiments in the A and B cores, ^{56}Fe, ^{27}Al, ^{115}In and ^{58}Ni were selected as activation foils (Table 1) to cover a fission spectrum (average 2 MeV and peak 0.7 MeV), and ^{197}Au was selected as a normalization factor for monitoring reactor power in the core. The reaction rate in the core was normalized by that of the ^{197}Au foil emitted by ^{197}Au(n, γ)^{198}Au in the core.   Foil dimensions in the center of the core (15, O; Fig. 1) were as follows: ^{56}Fe, ^{27}Al, ^{115}In and ^{58}Ni, $10 \times 10 \times 1$ mm^3; ^{197}Au, 8 mm diameter and 0.05 mm thick, and five foils were set at an axial central position as shown in Fig. 6a.   In the C-core, foil dimensions and variations in the center of the core (8, O; Fig. 3) were the same as in the B-core, and five foils were set at the central position in the axial direction as shown in Fig. 6b.   The neutron spectrum (Fig. 7) in the A-core was very hard at KUCA, whereas the B and C cores were almost the same as in well-thermalized ones and as in previous ADS experiments with 14 MeV neutrons (Pyeon et al., 2007; 2008).   The irradiation time of the activation foils and neutron flux level were one hour and 1×10^7 1/s/cm^2, respectively, in the critical experiments conducted in the three (A, B and C) cores.   The experimental error in each activation foil was estimated to be about 5% (Pyeon et al., 2009b), including detection efficiency, their self-shielding effect, the statistical error of γ-ray counts and the full width at half maximum (FWHM) of the γ-ray spectrum peak.

In the subcritical experiments, instead of ^{58}Ni used in the critical experiments, ^{93}Nb was

selected as the activation foil to cover a wide range of threshold energy of 14 MeV neutrons, besides ^{56}Fe, ^{27}Al and ^{115}In. ^{197}Au in the core and another ^{93}Nb at the target were selected as normalization factors for monitoring the reactor power and neutron source, respectively. The reaction rate experiments in the ADS with 14 MeV neutrons were carried out at subcriticality levels between 0.05 and 1.05 %$\Delta k/k$.   The measured subcriticality was obtained from the combination of the control and safety rod worth by the rod drop method and the control rod calibration curve by the positive period method.   Neutrons (14 MeV) generated by the D-T reactions were injected into a subcritical system under the following beam characteristics: 0.5 mA beam intensity; 40 Hz repetition rate; 5 μs pulsed width; 1.0×10^{8} 1/s neutron yield.

3. Experimental Analyses

3.1. Numerical Simulations

The numerical calculations were executed by the Monte Carlo transport code, MCNPX together with ENDF/B-VI.8 (Rose, 1991) and JENDL-3.3 (Shibata et al., 2002) for transport, and JENDL/D-99 (Kobayashi et al., 2002) for reaction rates.   Here, in MCNPX, the calculated reaction rate was obtained from the evaluation of the volume tallies of activation foils.   Although the effects of their reactivity are negligible, the foils were included in the simulated geometry and transport calculations.

The precision of numerical criticalities and subcriticalities in the eigenvalue calculations was attained within the relative difference of 5% between the results of the experiments and the calculations.   The eigenvalue calculation was executed for 1000 active cycles of 50,000 histories.   The subcriticalities in the eigenvalue calculation had statistical errors within 0.01 %$\Delta k/k$ and the reaction rates in critical and subcritical (the fixed-source) calculations were within 3%.

3.2. Critical Experiments

The experimental results of the reaction rates were obtained by measuring total counts of the peak energy of γ-ray emissions. The saturation activity D_∞ [1/s], which is proportional to the reaction rate [1/s/cm^3], taking into consideration the unit weight [g] of each foil and the density [g/cm^3], was calculated using the following equation:

$$D_\infty = \frac{\lambda T_c C (1+\alpha)}{\varepsilon \left(1-e^{-\lambda T_i}\right) \cdot e^{-\lambda T_w} \cdot \left(1-e^{-\lambda T_c}\right)} \quad , \tag{1}$$

where λ indicates the decay constant, T_c the measurement counting time, C the counting rate, α the internal conversion coefficient, ε the detection efficiency, T_i the irradiation time, and T_w the waiting time until the start of the measurement after the irradiation. Finally, the reaction rate was obtained from the saturation activity.

For the critical experiments in the B-core, a comparison (Table 2) between the experimental and the numerical values with ENDF-B-VI.8, JENDL-3.3 and JENDL/D-99 showed fairly good agreement for ^{115}In, ^{58}Ni and ^{27}Al with less than a relative difference of 6% of the C/E value, whereas ^{56}Fe still revealed a large discrepancy as obtained in the previous study. Here, the large discrepancy in the C/E value of ^{56}Fe was assumed to be caused by the composition ratio of material (foil): the purity of ^{56}Fe. The assumption was that ^{55}Mn (composition 0.5% in purity 99.5% ^{56}Fe; abundance ratio 100%) was activated by the absorption reactions ^{55}Mn(n, γ)^{56}Mn, and this ^{56}Mn material in ^{55}Mn(n, γ)^{56}Mn (Table 1) was considered to be generated coincidently in almost the same way as in ^{56}Fe(n, p)^{56}Mn reactions. Thus, the activity of ^{56}Mn was the results of induced by two reactions ^{55}Mn(n, γ)^{56}Mn and ^{56}Fe(n, p)^{56}Mn, and the experimental results were overestimated in the C/E evaluation of ^{56}Fe(n, p)^{56}Mn reactions. Under the calculation precision of ENDF/B-VI.8 in the B-core, the numerical analyses in the C and A cores were conducted by the combination of ENDF-B-VI.8 and JENDL/D-99.

8

On the basis of the assumption made in the B-core experiments, an additional critical experiment was carried out in the C-core. Foil dimensions were the same as in the B-core, and, six foils were employed as shown in Fig. 6b at position of (8, D) in Fig. 3. The neutron spectrum was as well thermalized as in the B-core. In the C-core, good accuracy (Table 3) of C/E values between the experiments and the calculations (ENDF-B-VI.8 and JENDL/D-99) was observed in the relative difference 8% at most for ^{115}In, ^{58}Ni, ^{27}Al and ^{56}Fe (purity 99.99%), whereas ^{56}Fe (purity 99.5%) still revealed a large discrepancy as seen in the B-core. From these results, ^{56}Fe (purity 99.99%) was considered improved as remarkably as the relative difference 5% of the C/E value in the comparison between the purity of 99.5% and 99.99% of ^{56}Fe, and the assumption mentioned in the B-core experiment was considered valid in the reaction rate analyses.

For confirming the purity issue through the experimental analyses, another critical experiment was carried out in the A-core. Foil dimensions were the same as those in the B-core, and, five foils were attached as shown in Fig. 6a at the position of (15, L) in Fig. 4. The neutron spectrum (Fig. 7) in the A-core was a hard one among the KUCA cores compared with the previous ADS experiments with 14 MeV neutrons and the current B-core. In the A-core, the relative difference (Table 4) between the experiments and the calculations (ENDF-B-VI.8 and JENDL/D-99) was found to be good around the relative difference 10% of the C/E value for all the foils (^{115}In, ^{58}Ni, ^{27}Al and ^{56}Fe of purity 99.99%).

From a series of critical experiments conducted at KUCA, the discrepancy in the C/E value of ^{56}Fe was attributable to the composition ratio of material ^{56}Fe, and the validity of the high purity of 99.99% of ^{56}Fe was considered cogent attaining the accuracy of reaction rate analyses in the experiments and calculations.

3.3. Subcritical Experiments with 14 MeV Neutrons

Before reaction rate analyses, a gold (Au) wire irradiation experiment was conducted in the A-core, under subcritical level 0.12 %$\Delta k/k$, to investigate the accuracy of reaction rate

analyses in the subcritical state.   The Au wire was set at position (11-19, Q-R) shown in Fig. 4, and numerical analyses of the Au reaction rates were conducted by using MCNPX with ENDF-B-VI.8 and JENDL/D-99.   The good agreement of reaction rates between the experiments and calculations demonstrated that the numerical precision of reaction rates was reliable enough in the subcritical states of the KUCA A-core, as shown in Fig. 8.

In the subcritical range between 0.05 and 1.05 %$\Delta k/k$, a comparison (Table 5 and Fig. 9) between the experiments and calculations (ENDF-B-VI.8 and JENDL/D-99) showed that the C/E values in ^{115}In and ^{56}Fe were fairly good around 10%, whereas those in ^{27}Al and ^{93}Nb were about 30%, with some exceptions, regardless of the subcriticality level.   The accuracy of experimental and numerical reaction rates was considered to be remarkably improved, as compared with that in previous ADS experiments with 14 MeV neutrons, demonstrating the validity of selecting ^{56}Fe with a purity of 99.99% in the subcritical experiments and the precision of numerical analyses by using MCNPX together with ENDF/B-VI.8 and JENDL/D-99.   On the other hand, when the subcriticality level was deep, the C/E values in ^{115}In, ^{56}Fe and ^{27}Al were observed to be approximately constant under the subcritical level ranging between 0.05 and 1.05 %$\Delta k/k$.   In short, for ^{115}In, ^{56}Fe and ^{27}Al, the subcriticality dependence was not found in the reaction rate analyses up to subcritical level 1.05 %$\Delta k/k$. Inversely, in case of ^{93}Nb, the reaction rate analyses in the subcritical systems were still found to be dependent on subcriticality as in the previous study.   From these results, a remarkable improvement of reaction rates was successfully accomplished by excluding the effects of uncertainty factors, including the small size of activation foils and the large perturbation in the core, as much as possible.

4. Conclusions

Reaction rate experiments were carried out at KUCA to evaluate the accuracy of experiments and calculations under the subcritical states.   A comparison between the

experiments and the calculations by MCNPX with ENDF/B-VI.8 and JENDL/D-99 revealed the following:

Before subcritical experiments, critical experiments on the reaction rates of ^{115}In, ^{56}Fe, ^{27}Al and ^{58}Ni foils were carried out in the A, B and C cores by the foil activation method, and the C/E values between the experiments and the calculations were almost within the relative difference of 10％．In the critical experimental analyses, special mention should be made of the remarkable effect of the composition ratio of material ^{56}Fe: the remarkable improvement of the large discrepancy between the experimental and numerical reaction rates by selecting ^{56}Fe with a purity of 99.99％.

For the ADS experiments with 14 MeV neutrons, the C/E value between the experiments and the calculations was found to be well within the relative difference of about 30% in all foils, ranging between subcriticality 0.05 and 1.05 %$\Delta k/k$. Furthermore, another remarkable effect attained was that no dependence of the reaction rates on the subcriticality level, in cases of ^{115}In, ^{56}Fe, ^{27}Al, was found, whereas subcriticality dependence was observed in the reaction rates of ^{93}Nb.

References

Gohar, Y., Aliberti, G., Bolshinsky, I., et al., 2009. YALINA-booster subcritical assembly conversion. Trans. Am. Nucl. Soc., 101, 39-40.

Hendricks, J.S., McKinney, G.W., Waters, L.S. et al., 2005. MCNPX user's manual, version 2.5.0.," LA-UR-05-2675, Los Alamos National Laboratory.

Kobayashi, K., Iguchi, T., Iwasaki, S., et al., 2002. JENDL dosimetry file 99 (JENDL/D-99). JAERI Report 1344.

Lebrat, J.F., Aliberti, G., D'Angelo, A., et al., 2008. Global results from deterministic and stochastic analysis of the MUSE-4 experiments on the neutronics of the accelerator-driven systems. Nucl. Sci. Eng., 158, 49-67.

Nishihara, K., Iwanaga, K., Tsujimoto, K., et al., 2008. Neutronics design of accelerator-driven system for power flattening and beam current reduction. J. Nucl. Sci. Technol., 45 812-822.

Persson, C.M., Fokau, A., Serafimovich, I., et al., 2008. Pulsed neutron source measurements in the subcritical ADS experiment YALINA-Booster, Ann. Nucl. Energy, 35, 2357-2364.

Plaschy, M., Destouches, C., Rimpault, G., et al., 2005. Investigation of ADS-type heterogeneities in the MUSE4 critical configuration. J. Nucl. Sci. Technol., 42, 779-787.

Pyeon, C.H., Shiga, H., Abe, K., et al., 2010. Reaction rate analysis of nuclear spallation reactions generated by 150, 190 and 235 MeV protons. J. Nucl. Sci. Technol., 47, 1090-1095.

Pyeon, C.H., Misawa, T., Lim, J.Y., et al., 2009a. First injection of spallation neutrons generated by high-energy protons into the Kyoto University Critical Assembly. J. Nucl. Sci. Technol., 46, 1091-1093.

Pyeon, C.H., Shiga, H., Misawa, T., et al., 2009b. Reaction rate analyses for an accelerator-driven system with 14 MeV neutrons in the Kyoto University Critical Assembly. J. Nucl. Sci. Technol., 46, 965-972.

Pyeon, C.H., Hervault, M., Misawa, T., et al., 2008. Static and kinetic Experiments on accelerator-driven system in Kyoto University Critical Assembly. J. Nucl. Sci.

Technol., 45, 1171-1182.

Pyeon, C.H., Hirano, Y., Misawa, T., et al., 2007. Preliminary experiments on accelerator-driven subcritical reactor with pulsed neutron generator in Kyoto University Critical Assembly. J. Nucl. Sci. Technol., 44, 1368-1378.

Pyeon, C.H., Misawa, T., Shiroya, S., et al., 2004. Experiments and analyses for relationship between flux tilt in two-energy-group model and eigenvalue separation. J. Nucl. Sci. Technol., 41, 171-176.

Rose, P.F., 1991. ENDF-201, ENDF/B-VI summary documentation. BNL-NCS-17541, 4th edition.

Rubbia, C., 1995. A high gain energy amplifier operated with fast neutrons. In: AIP Conference Proceedings, 346, 44-53; see also 1994. In: Proceedings of International Conference on Accelerator-Driven Transmutation Technologies and Application, Las Vegas, July 25-29.

Shibata, K., Kawano, T., Nakagawa, T., et al., 2002. Japanese evaluated nuclear data library version 3 revision-3: JENDL-3.3. J. Nucl. Sci. Technol., 39, 1125.

Soule, R., Assal, W., Chaussonnet, P., et al., 2004. Neutronic studies in support of accelerator-driven systems: The MUSE experiments in the MASURCA facility. Nucl. Sci. Eng., 148, 124-152.

Sugawara, T., Nishihara, K., Tsujimoto, K., et al., 2010. Analytical validation of uncertainty in reactor physics parameters for nuclear transmutation systems. J. Nucl. Sci. Technol., 47, 521-530.

Sugawara, T., Sarotto, M., Stankovskiy A., et al., 2011. Nuclear data sensitivity/uncertainty analysis for XT-ADS. Ann. Nucl. Energy, 38, 1098-1108.

Taninaka, H., Hashimoto, K., Pyeon, C.H., et al., 2011. Determination of subcritical reactivity of a thermal accelerator-driven system from beam trip and restart experiment. J. Nucl. Sci. Technol., 48, 873-879.

Taninaka, H., Hashimoto, K., Pyeon, C.H., et al., 2010. Determination of lambda-mode

eigenvalue separation of a thermal accelerator-driven system from pulsed neutron experiment. J. Nucl. Sci. Technol., 47, 376-383.

Tesinsky, M., Berglöf, C., Bäck, T., et al., 2011. Comparison of calculated and measured reaction rates obtained through foil activation in the subcritical dual spectrum facility YALINA-Booster, Ann. Nucl. Energy, 38, 1412-1417.

Uyttenhove, W., Baeten, P., Van den Eyde, G., et al., 2011. The neutronic design of a critical lead reflected zero-power reference core for on-line subcriticality measurements in accelerator-driven systems. 38, 1519-1526.

Xia, H.H., 2009. The progress of researches on ADS in China. ICFA Beam Dynamics Newsletter, 49, 72-80.

X-5 Monte Carlo Team, 2005. MCNP – A general Monte Carlo N-particle transport code, version 5. LA-UR-03-1987

Table captions

Table 1   Main characteristics of activation foils used in the critical and subcritical

experiments

Table 2   C/E values of measured and calculated reaction rates in the critical state (B-core)

Table 3   C/E values of measured and calculated reaction rates in the critical state (C-core)

Table 4   C/E values of measured and calculated reaction rates in the critical state (A-core)

Table 5   C/E values of measured and calculated reaction rates in the subcritical states

(A-core)

Table 1   Main characteristics of activation foils used in the critical and subcritical experiments

Reaction	Threshold [MeV]	Half-life	γ-ray energy [keV]	Emission rate [%]
^{115}In (*n, n'*) ^{115m}In	0.32	4.489 h	336.2	45.8
^{58}Ni (*n, p*) ^{58}Co	0.90	70.82 d	810.8	99.4
^{56}Fe (*n, p*) ^{56}Mn	2.97	2.578 h	846.8	98.9
			1810.7	27.2
			2113.1	14.3
^{27}Al (*n, α*) ^{24}Na	3.25	14.96 h	1368.6	100
			2754.1	99.9
^{93}Nb (*n, 2n*) ^{92m}Nb	8.9	10.15 d	934.3	99.9
^{197}Au (*n, γ*) ^{198}Au	-	2.695 d	411.8	95.5
^{55}Mn (*n, γ*) ^{56}Mn	-	2.578 h	846.8	98.9
			1810.7	27.2
			2113.1	14.3

Table 2 C/E values of measured and calculated reaction rates in the critical state (B-core)

Reaction	Measured reaction rate [1/s/cm^3]	C/E value	
		ENDF/B-VI.8 JENDL/D-99	JENDL-3.3 JENDL/D-99
^{115}In (n, n') ^{115m}In	$(7.36 \pm 0.06) \times 10^5$	0.98 ± 0.01	0.99 ± 0.01
^{58}Ni (n, p) ^{58}Co	$(7.11 \pm 0.03) \times 10^5$	0.95 ± 0.01	0.94 ± 0.01
^{56}Fe (n, p) ^{56}Mn (*)	$(3.03 \pm 0.01) \times 10^5$	0.03 ± 0.01	0.03 ± 0.01
^{27}Al (n, α) ^{24}Na	$(4.57 \pm 0.01) \times 10^5$	1.02 ± 0.03	0.96 ± 0.02
^{197}Au (n, γ) ^{198}Au	$(5.81 \pm 0.02) \times 10^8$	-	-

(*): Purity 99.5%

Table 3 C/E values of measured and calculated reaction rates in the critical state (C-core)

Reaction	Purity (%)	Measured reaction rate [1/s/cm^3]	C/E value (ENDF/B-VI.8 JENDL/D-99)
^{115}In (n, n') ^{115m}In	-	$(1.25 \pm 0.01) \times 10^5$	0.93 ± 0.01
^{58}Ni (n, p) ^{58}Co	-	$(1.14 \pm 0.01) \times 10^5$	0.94 ± 0.01
^{56}Fe (n, p) ^{56}Mn	99.5	$(3.67 \pm 0.02) \times 10^4$	0.04 ± 0.01
^{56}Fe (n, p) ^{56}Mn	99.99	$(1.43 \pm 0.02) \times 10^3$	0.95 ± 0.02
^{27}Al (n, α) ^{24}Na	-	$(6.44 \pm 0.02) \times 10^2$	1.08 ± 0.04
^{197}Au (n, γ) ^{198}Au	-	$(9.35 \pm 0.04) \times 10^7$	-

Table 4 C/E values of measured and calculated reaction rates in the critical state (A-core)

Reaction	Measured reaction rate [1/s/cm^3]	C/E value (ENDF/B-VI.8 JENDL/D-99)
^{115}In (n, n') ^{115m}In	$(2.11 \pm 0.02) \times 10^5$	0.87 ± 0.02
^{58}Ni (n, p) ^{58}Co	$(1.58 \pm 0.01) \times 10^5$	1.00 ± 0.02
^{56}Fe (n, p) ^{56}Mn (**)	$(1.99 \pm 0.02) \times 10^3$	0.94 ± 0.03
^{27}Al (n, α) ^{24}Na	$(9.86 \pm 0.18) \times 10^2$	1.07 ± 0.04
^{197}Au (n, γ) ^{198}Au	$(5.92 \pm 0.02) \times 10^7$	1.07 ± 0.04

(**): Purity 99.99%

Table 5 C/E values of measured and calculated (ENDF/B-VI.8 and JENDL/D-99) reaction rates in subcritical states (A-core)

| Reaction	Subcriticality [%$\Delta k/k$]				
	0.05	0.12	0.27	0.59	1.05
^{115}In (n, n') ^{115m}In	0.92 ± 0.01	0.94 ± 0.01	0.91 ± 0.01	0.89 ± 0.01	0.96 ± 0.02
^{56}Fe (n, p) ^{56}Mn (**)	1.10 ± 0.02	1.08 ± 0.02	1.04 ± 0.02	1.01 ± 0.02	1.03 ± 0.03
^{27}Al (n, α) ^{24}Na	1.32 ± 0.02	1.27 ± 0.02	1.31 ± 0.03	1.27 ± 0.04	1.35 ± 0.05
^{93}Nb $(n, 2n)$ ^{92m}Nb	1.66 ± 0.05	1.24 ± 0.08	1.17 ± 0.13	1.10 ± 0.11	1.26 ± 0.06

(**): Purity 99.99%

Figure captions

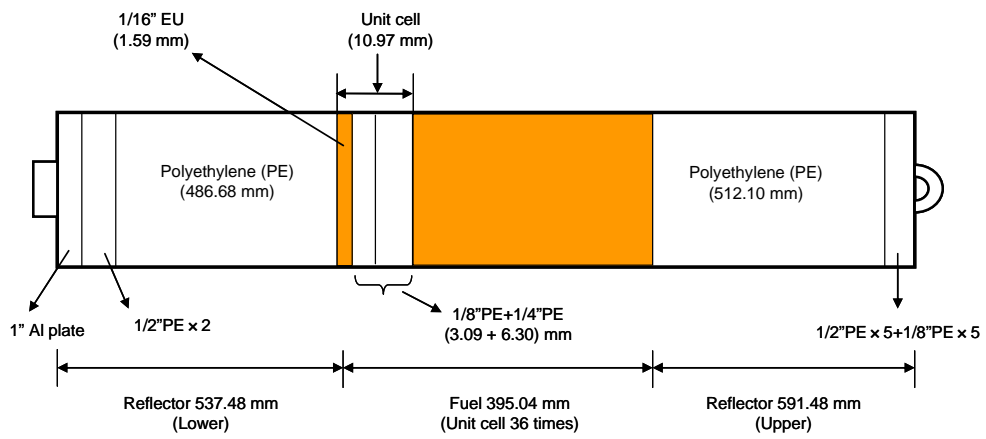Fig. 1   Top view of the KUCA B-core (B3/8"P36EU(3)) in the critical experiment

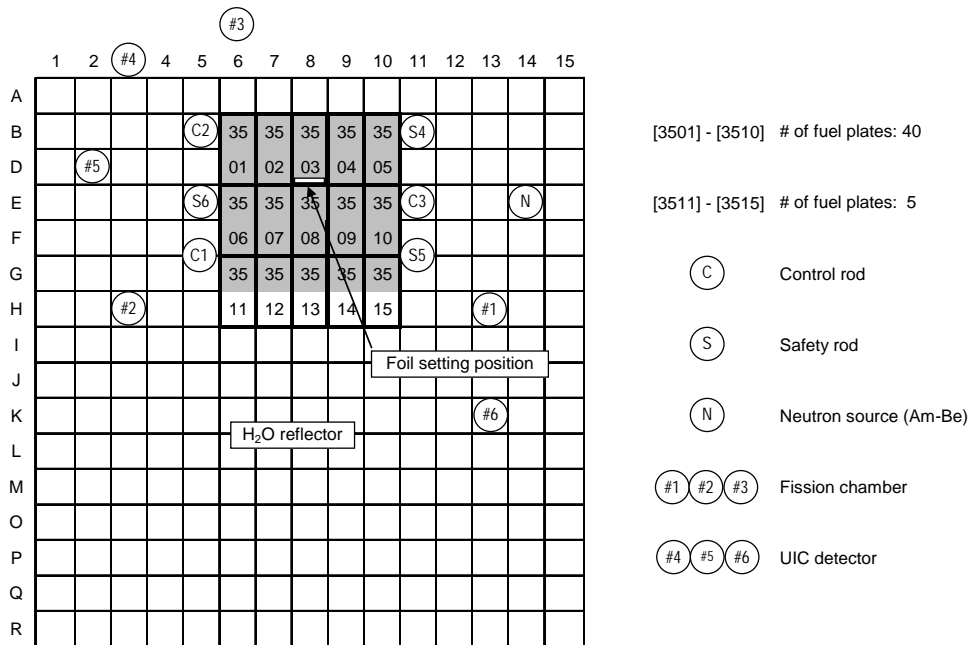Fig. 2   Schematic drawing of the 3/8P"36EU fuel assembly (F; Fig. 1) in the B-core

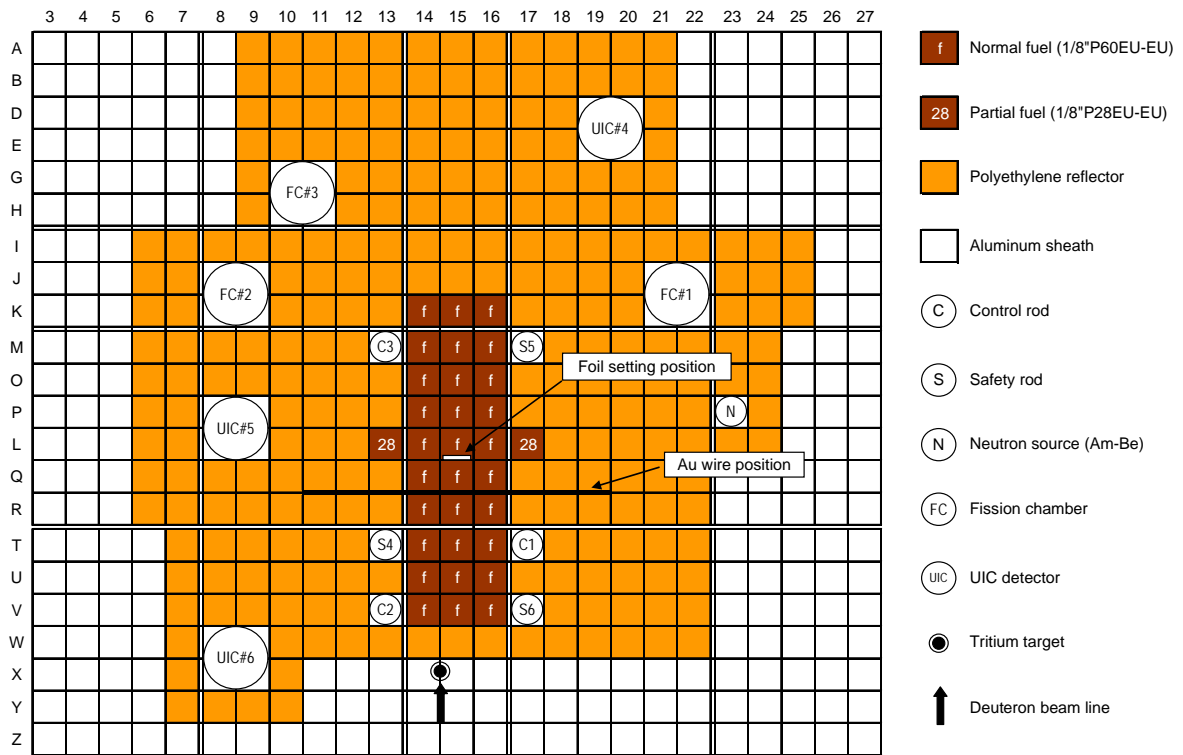Fig. 3   Top view of the KUCA C-core (C35G0(5))

Fig. 4   Top view of the KUCA A-core (A1/8"P60EU-EU(3)) in critical and subcritical experiments

Fig. 5   Schematic drawings of fuel assemblies in the A-core (a) 1/8"P60EU-EU fuel assembly (f; Fig. 4) and (b) 1/8"P28EU-EU (28; Fig. 4)

Fig. 6   Activation foils setting at fuel assemblies (a) (15, O) of the B-core in Fig. 1 and (15, L) of the A-core in Fig. 4 (Fe, Al, In and x: $10 \times 10 \times 1$ mm^3; Au: 8 mm dia. and 0.05 mm thick; x is Ni and Nb in critical and subcritical experiments, respectively) and (b) (8, D) of the C-core in Fig. 3 (Fe, Al, In and Ni: $10 \times 10 \times 1$ mm^3; Au: 8 mm dia. and 0.05 mm thick; Fe_L: purity 99.5%, Fe_H: purity 99.99%)

Fig. 7   Neutron spectra at (15, L) in the A-core and (15, O) in the B-core

Fig. 8   Comparison between measured and calculated Au reaction rate distributions in the subcritical state ($\rho = 0.12$ %$\Delta k/k$) of the A-core

Fig. 9   Comparison between the C/E values of reaction rates in experiments and calculations (Table 5) for subcriticality (MeV values in parentheses indicate the threshold energy of each foil.)
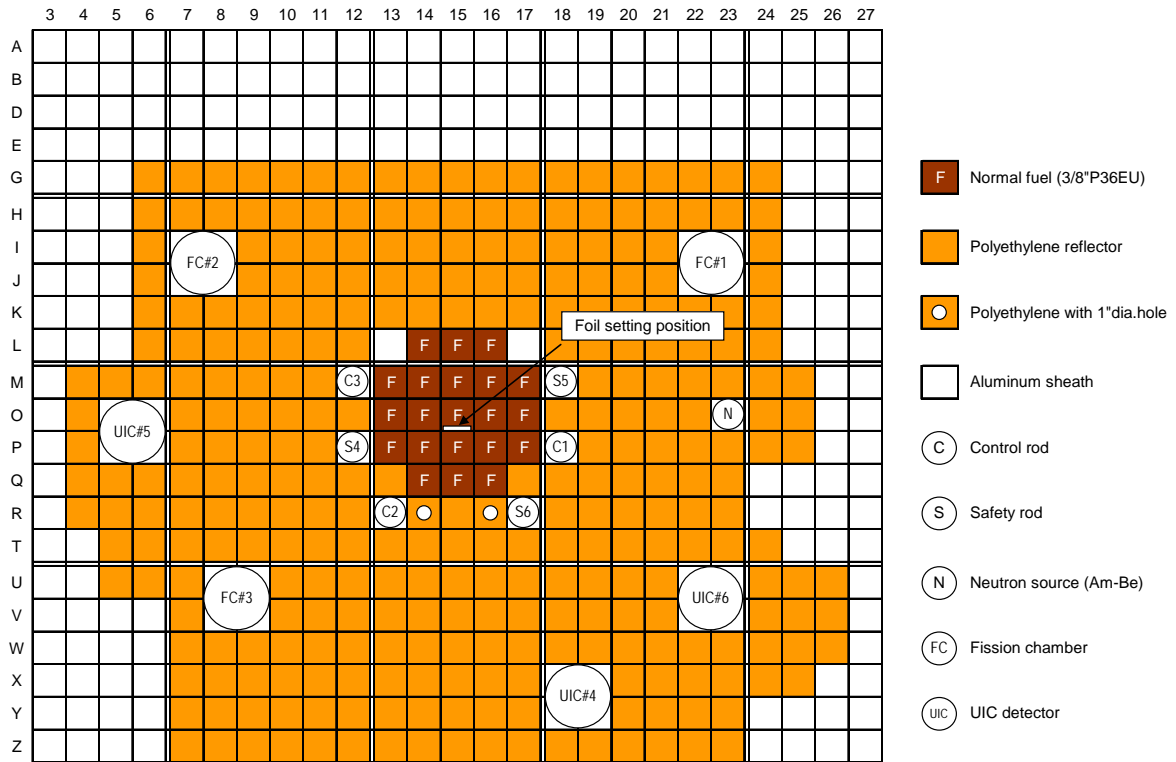
Fig. 1   Top view of the KUCA B-core (B3/8"P36EU(3)) in the critical experiment

Fig. 2　Schematic drawing of the 3/8P"36EU fuel assembly (F; Fig. 1) in the B-core
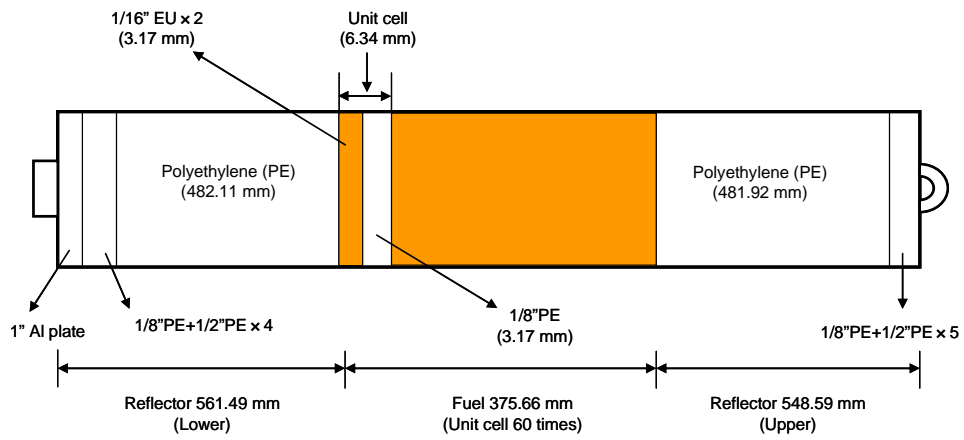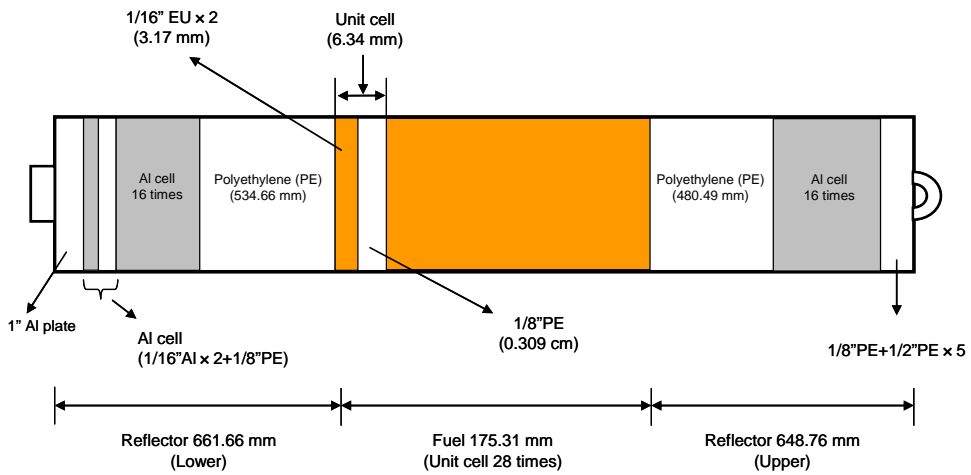
Fig. 3   Top view of the KUCA C-core (C35G0(5))

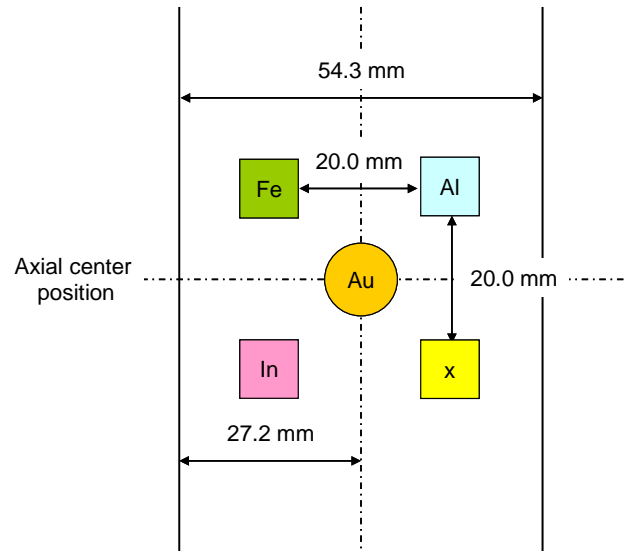Fig. 4 Top view of the KUCA A-core (A1/8"P60EU-EU(3)) in critical and subcritical experiments
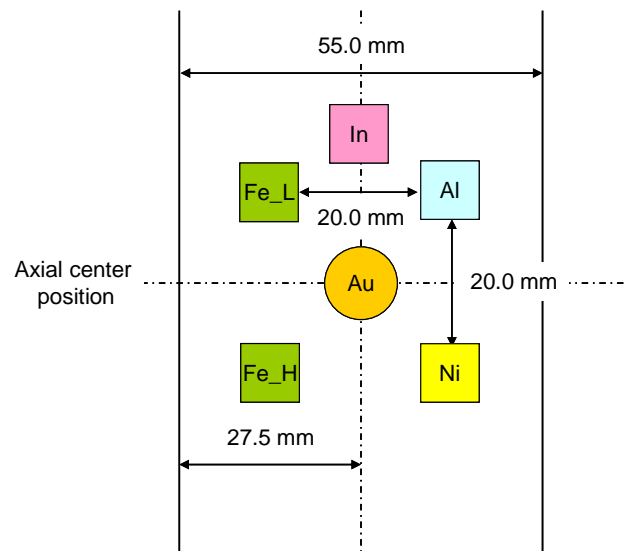
(a) 1/8"P60EU-EU fuel assembly (f; Fig. 4)

(b) 1/8"P28EU-EU fuel assembly (28; Fig. 4)

Fig. 5   Schematic drawings of fuel assemblies in the A-core

(a) (15, O) of the B-core in Fig. 1 and (15, L) of the A-core in Fig. 4 (Fe, Al, In and x: $10\times10\times1$ mm³; Au: 8 mm dia. and 0.05 mm thick; x is Ni and Nb in critical and subcritical experiments, respectively)

(b) (8, D) of the C-core in Fig. 3 (Fe, Al, In and Ni: $10\times10\times1$ mm³; Au: 8 mm dia. and 0.05 mm thick; Fe_L: purity 99.5%, Fe_H: purity 99.99%)
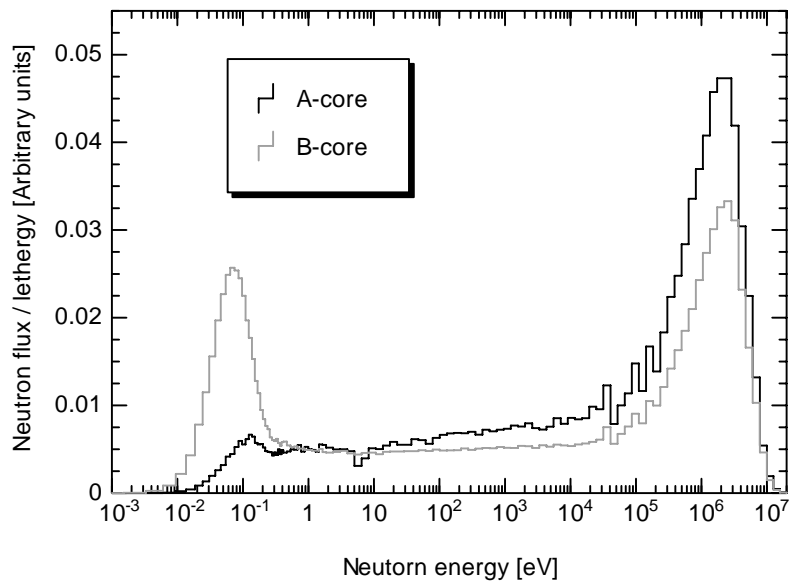
Fig. 6   Activation foils setting at fuel assemblies

Fig. 7   Neutron spectra at (15, L) in the A-core and (15, O) in the B-core
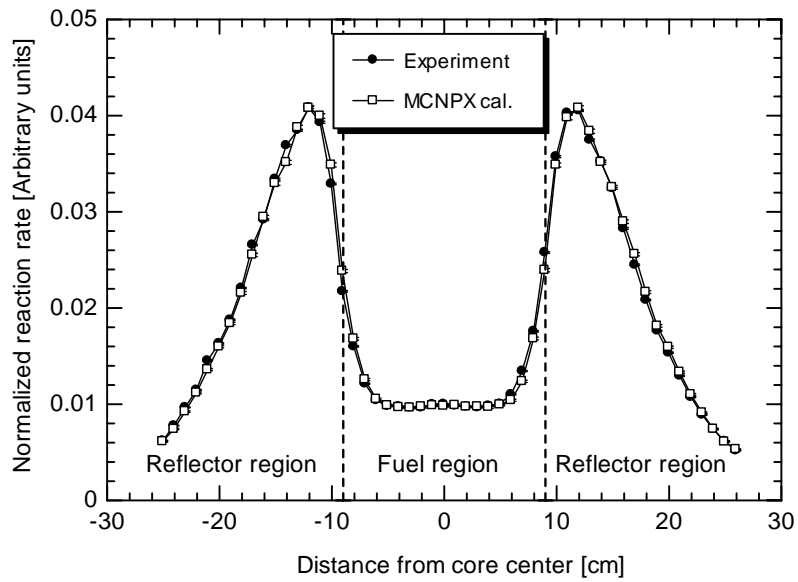
Fig. 8   Comparison between measured and calculated Au reaction rate distributions in the subcritical state ($\rho = 0.12$ %$\Delta k/k$) of the A-core
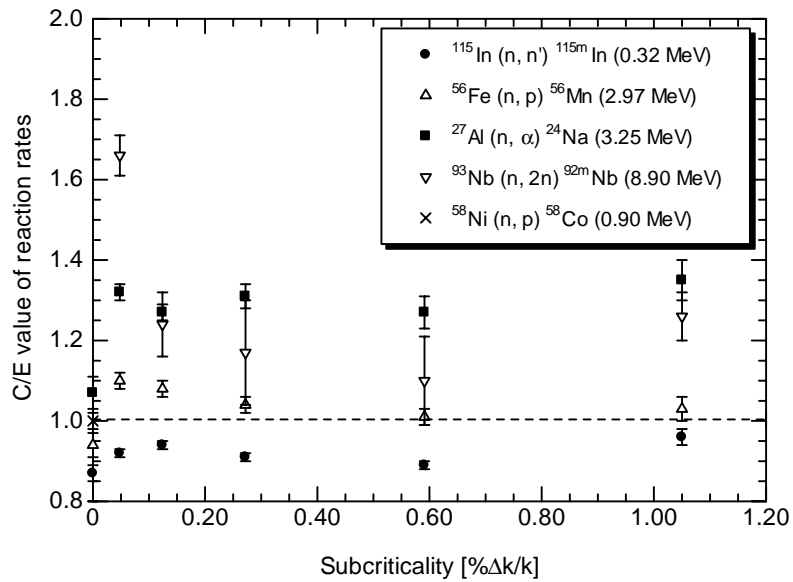
Fig. 9 Comparison between the C/E values of reaction rates in experiments and calculations (Table 5) for subcriticality (MeV values in parentheses indicate the threshold energy of each foil.)